Online Research @ Cardiff

This is an Open Access document downloaded from ORCA, Cardiff University's institutional repository: https://orca.cardiff.ac.uk/id/eprint/104380/

This is the author's version of a work that was submitted to / accepted for publication.

Citation for final published version:

Marshall, Jonathan P., Booth, Mark, Holland, Wayne, Matthews, Brenda C., Greaves, Jane ORCID: https://orcid.org/0000-0002-3133-413X and Zuckerman, Ben 2016. Far-infrared and sub-millimetre imaging of HD 76582's circumstellar disc. Monthly Notices of the Royal Astronomical Society 459 (3) , pp. 2893-2904. 10.1093/mnras/stw813 file

Publishers page: http://dx.doi.org/10.1093/mnras/stw813 <http://dx.doi.org/10.1093/mnras/stw813>

Please note:
Changes made as a result of publishing processes such as copy-editing, formatting and page numbers may not be reflected in this version. For the definitive version of this publication, please refer to the published source. You are advised to consult the publisher's version if you wish to cite this paper.

This version is being made available in accordance with publisher policies. See http://orca.cf.ac.uk/policies.html for usage policies. Copyright and moral rights for publications made available in ORCA are retained by the copyright holders.

information services
gwasanaethau gwybodaeth

Monthly Notices
of the
ROYAL ASTRONOMICAL SOCIETY

MNRAS **459,** 2893–2904 (2016)
Advance Access publication 2016 April 8

doi:10.1093/mnras/stw813

Far-infrared and sub-millimetre imaging of HD 76582's circumstellar disc

Jonathan P. Marshall,[1,2]★ Mark Booth,[3] Wayne Holland,[4,5] Brenda C. Matthews,[6,7] Jane S. Greaves[8] and Ben Zuckerman[9]

[1]*School of Physics, UNSW Australia, High Street, Kensington, Sydney, NSW 2052, Australia*
[2]*Australian Centre for Astrobiology, UNSW Australia, High Street, Kensington, Sydney, NSW 2052, Australia*
[3]*Instituto de Astrofísica, Pontificia Universidad Católica de Chile, Vicua Mackenna 4860, 7820436 Macul, Santiago, Chile*
[4]*UK Astronomy Technology Center, Royal Observatory, Blackford Hill, Edinburgh EH9 3HJ, UK*
[5]*Institute for Astronomy, University of Edinburgh, Royal Observatory, Blackford Hill, Edinburgh EH9 3HJ, UK*
[6]*National Research Council of Canada, 5071 West Saanich Road, Victoria, BC V9E 2E7, Canada*
[7]*University of Victoria, Finnerty Road, Victoria, BC V8W 3P6, Canada*
[8]*School of Physics and Astronomy, Cardiff University, Queen's Buildings, The Parade, Cardiff CF24 3AA, UK*
[9]*Department of Physics and Astronomy, University of California, Los Angeles, CA 90095, USA*

Accepted 2016 April 5. Received 2016 April 3; in original form 2016 February 29

ABSTRACT

Debris discs, the tenuous rocky and icy remnants of planet formation, are believed to be evidence for planetary systems around other stars. The JCMT/SCUBA-2 debris disc legacy survey 'SCUBA-2 Observations of Nearby Stars' (SONS) observed 100 nearby stars, amongst them HD 76582, for evidence of such material. Here, we present imaging observations by JCMT/SCUBA-2 and *Herschel*/PACS at sub-millimetre and far-infrared wavelengths, respectively. We simultaneously model the ensemble of photometric and imaging data, spanning optical to sub-millimetre wavelengths, in a self-consistent manner. At far-infrared wavelengths, we find extended emission from the circumstellar disc providing a strong constraint on the dust spatial location in the outer system, although the angular resolution is too poor to constrain the interior of the system. In the sub-millimetre, photometry at 450 and 850 μm reveals a steep fall-off that we interpret as a disc dominated by moderately sized dust grains ($a_{\rm min} = 36\,\mu$m), perhaps indicative of a non-steady-state collisional cascade within the disc. A disc architecture of three distinct annuli, comprising an unresolved component at 20 au and outer components at 80 and 270 au, along with a very steep particle size distribution ($\gamma = 5$), is proposed to match the observations.

Key words: circumstellar matter – stars: individual: HD 76582 – planetary systems.

1 INTRODUCTION

The presence of a circumstellar dust disc around a mature, main-sequence star is interpreted as a visible signpost of a planetary system (Matthews et al. 2014). These discs are the remnants of asteroidal and cometary bodies broken up in mutual collisions and so are commonly known as 'debris discs' (Backman & Paresce 1993; Krivov 2010). Debris discs comprise icy and rocky bodies ranging from sub-micron-sized dust grains to kilometre-sized planetesimals, analogous to the Solar system's Asteroid belt and Edgeworth–Kuiper belt (Wyatt 2008). Between 20 and 30 per cent of nearby, main-sequence AFGK-type stars have been identified as hosting cool debris discs, with fractional luminosities ($L_{\rm IR}/L_\star$) ranging from 10^{-3} to 10^{-6} (Eiroa et al. 2013; Thureau et al. 2014). The observed disc incidence is sensitivity limited, with current instrumentation unable to directly detect a disc of equivalent brightness to the Edgeworth–Kuiper belt around another star ($L_{\rm IR}/L_\star \sim 1.2 \times 10^{-7}$; Vitense et al. 2012). Understanding these structures is fundamental to obtaining a full picture of the outcomes of planet formation processes, and the evolution of planetary systems (e.g. Marshall et al. 2014a; Moro-Martín et al. 2015; Wittenmyer & Marshall 2015).

The debris disc around HD 76582 was identified by detection of infrared excess from the star at 60 μm in the all-sky survey by the *InfraRed Astronomical Satellite* (*IRAS*; Neugebauer et al. 1984). Its fractional luminosity of $1.7 \pm 0.2 \times 10^{-4}$, estimated from a single-temperature blackbody fitted with a temperature of 80 K (Zuckerman & Song 2004b; Moór et al. 2006), is consistent with a steady-state collisional cascade according to the evolutionary models of Dominik & Decin (2003) assuming an age of ∼0.5 Gyr (Moór et al. 2006; Rhee et al. 2007; David & Hillenbrand 2015). However, if the age of ∼2 Gyr from Zorec & Royer (2012) is considered, then the disc appears to be unusually bright.

★E-mail: jonty.marshall@unsw.edu.au

© 2016 The Authors
Published by Oxford University Press on behalf of the Royal Astronomical Society

Downloaded from https://academic.oup.com/mnras/article-abstract/459/3/2893/2595210/Far-infrared-and-sub-millimetre-imaging-of-HD
by Cardiff University user
on 06 September 2017

Images at longer wavelengths trace larger and colder dust grains, making them useful in identifying the location of the dust producing planetesimal belts around a disc-host star (Krivov et al. 2008). Additionally, (sub-)millimetre wavelength observations are ideal for probing asymmetric structures formed by resonance-trapped dust grains in discs, possibly caused by perturbing planets (e.g. Wyatt 2003; Hughes et al. 2011; Lestrade & Thilliez 2015). In the case of HD 76582, the data presented here are low signal-to-noise ratio (S/N; 5–10-σ integrated detection) and the disc is unresolved. The sub-millimetre data are critical to the disc modelling process, constraining the dust particle size distribution from the SED's sub-millimetre slope for the first time, and providing a measure of the dust mass in the system.

The *Spitzer*/IRS spectrum, spanning mid-infrared wavelengths, reveals the presence of a second, warm component to this disc (Chen et al. 2014). Debris discs with spectral energy distributions (SEDs) exhibiting two distinct temperatures are inferred to comprise two physically distinct planetesimal rings that produce the dust at different temperatures (Morales et al. 2011). A favoured mechanism invoked for keeping the space between the two planetesimal rings free of migrating dust is the presence of one (or more) planet(s) (Su et al. 2013). Determination of the architectures of these systems solely from their SEDs is limited by the contrast between the warm and cool dust components (Kennedy & Wyatt 2014). Such interpretation is crude, and even combining the SED with moderately resolved disc images cannot always provide a clear architecture from modelling (e.g. Ertel et al. 2014). High angular resolution images are therefore critical to interpretation of these systems.

In this work we combine these disparate data to produce a self-consistent and coherent model of the disc's architecture and evolutionary state. In Section 2 we present the observations used to model this system, including the new SCUBA-2 sub-millimetre images and ancillary data from the literature. In Section 3 we present a summary of the simultaneous modelling of imaging and photometric data. In Section 4 we discuss the outcomes of the modelling process, interpreting the properties of HD 76582's disc as part of the ensemble of known debris discs. Finally in Section 5 we present our conclusions.

2 OBSERVATIONS

Here, we summarize the stellar physical parameters and the available photometric measurements of the HD 76582 system. These were taken from a variety of literature sources and combined with new data from the *Herschel*/PACS and JCMT/SCUBA-2 observations in the modelling process.

2.1 Stellar parameters and photosphere

HD 76582 (HIP 44001, o^2 Cnc) is an F0 IV type star located at a distance of 46.13 $\pm$ 0.69 pc. The distance was taken from the re-reduction of *HIPPARCOS* data by van Leeuwen (2007). The spectral type is taken from Skiff (2014). Studies have found no evidence of binarity or multiplicity for the system (Eggleton & Tokovinin 2008; De Rosa et al. 2014). The absolute magnitude and bolometric correction are taken from Ammler-von Eiff & Reiners (2012). The effective temperature, $T_{\rm eff}$, surface gravity, $\log g$, stellar radius, $R_\star$, and stellar mass, $M_\star$, are taken from Allende Prieto & Lambert (1999). The metallicity, [Fe/H], is taken from Giridhar et al. (2013). The rotational velocity $v \sin i$ and the rotational period (modulo the unknown stellar inclination) $P_{\rm rot}/\sin i$ are taken from Ammler-von Eiff & Reiners (2012). Stellar age estimates in the literature range from 300 Myr, based on *UVW* space velocities (Zuckerman & Song 2004a) and HR diagram location (Lowrance et al. 2000), or 450^{+150}_{-290} Myr (Moór et al. 2006), to 2.13 $\pm$ 0.24 Gyr (Zorec & Royer 2012). The stellar physical parameters used in this work are summarized in Table 1.

Table 1. Stellar physical properties.

Parameter	HD 76582
Distance (pc)	46.13 ± 0.69
Right Ascension[a] (h:m:s)	$08^{\rm h}57^{\rm m}35\overset{\rm s}{.}200$
Declination[a] (d:m:s)	$+15^\circ34'52\overset{''}{.}61$
Spectral type	F0 IV
V, $B-V$ (mag)	5.687, 0.207
M_V, B.C.[b] (mag)	2.580, −0.03
$L_\star$ ($L_\odot$)	10.30 ± 0.43
$T_{\rm eff}$ (K)	7868
$\log g$ (cm/s^2)	4.25
$R_\star$ ($R_\odot$)	1.62 ± 0.08
$M_\star$ ($M_\odot$)	1.72 ± 0.01
[Fe/H]	0.2
$v \sin i$ (km/s)	90.5 ± 4.5
$P_{\rm rot}/\sin i$ (d)	0.8
Age (Gyr)	0.30 to 2.13

Notes: (a) Coordinates are in ICRS J2000 epoch (b) bolometric correction.

A Kurucz stellar photosphere model (Castelli & Kurucz 2004) was scaled to the optical (Perryman et al. 1997; Hauck & Mermilliod 1998), near- and mid-infrared (Skrutskie et al. 2006; Egan et al. 2003; Wright et al. 2010) measurements at wavelengths <15 μm (where no clear excess is visible) using a least-squares fit to the measured flux densities, weighted by their individual uncertainties. The best-fitting model was subsequently extrapolated into the far-infrared and sub-millimetre in order to quantify the stellar contribution to the total emission at those longer wavelengths.

2.2 Photometry and spectroscopy

In addition to the sub-millimetre images and photometry from JCMT/SCUBA-2, we compiled literature photometry spanning the mid- and far-infrared to characterize the debris disc's thermal emission. Of particular note are the mid-infrared *Spitzer*/IRS spectrum and far-infrared *Herschel*/PACS images, both of which provide complementary data, namely tracing the rise of the disc emission above the stellar photosphere, and the peak emission and spatial extent of the disc, respectively. These measurements are critical to obtaining a comprehensive overview of the disc architecture. A summary of the photometry used in modelling the star and debris disc is presented in Table 2.

2.2.1 *Mid-infrared*

We use the *MSX* (Egan et al. 2003), *AKARI* (Ishihara et al. 2010), and *WISE* (Wright et al. 2010) photometry to constrain the mid-infrared SED. A *Spitzer* (Werner et al. 2004) InfraRed Spectrograph (IRS; Houck et al. 2004) observation of HD 76582 (Program ID 40651, P.I. Houck) spanning 5 to 38 μm was obtained from the CASSIS archive[1] (Lebouteiller et al. 2011). The spectrum was scaled to the stellar photosphere model between 8 and 12 μm by least-squares fitting. A factor of 1.04 (increase of 4 per cent) was applied to

[1] The Cornell Atlas of *Spitzer*/IRS Sources (CASSIS) is a product of the Infrared Science Center at Cornell University, supported by NASA and JPL.

Downloaded from https://academic.oup.com/mnras/article-abstract/459/3/2893/2595210/Far-infrared-and-sub-millimetre-imaging-of-HD
by Cardiff University user
on 06 September 2017

Table 2. Photometry used in modelling.

Wavelength (μm)	Flux density (mJy)	Telescope and instrument	Reference
0.349	5555 ± 15	Strömgren *u*	1
0.411	17290 ± 64	Strömgren *v*	1
0.440	17710 ± 81	Johnson *B*	2
0.466	20340 ± 75	Strömgren *b*	1
0.546	19720 ± 181	Strömgren *y*	1
0.550	19180 ± 179	Johnson *V*	2
0.790	16070 ± 147	Cousins *I*	2
1.235	12430 ± 261	2MASS *J*	3
1.662	8455 ± 139	2MASS *H*	3
2.159	5623 ± 123	2MASS K_S	3
4.29	1538 ± 149	*MSX* B1	4
4.35	1496 ± 156	*MSX* B2	4
4.60	1742 ± 130	*WISE* W2	5
8.28	463 ± 24	*MSX* A	4
9.0	392 ± 30	*AKARI*/IRC	6
11.6	262 ± 4	*WISE* W3	5
12.13	217 ± 15	*MSX* C	4
13.0	201 ± 14	*Spitzer*/IRS	7
14.65	151 ± 13	*MSX* D	4
18.0	121 ± 12	*Spitzer*/IRS	7
22.1	93 ± 3	*WISE* W4	5
24.0	87 ± 9	*Spitzer*/IRS	7
31.0	87 ± 15	*Spitzer*/IRS	7
60.0	391 ± 47	*IRAS* 60	8
100.0	609 ± 43	*Herschel*/PACS	7
160.0	495 ± 35	*Herschel*/PACS	7
450.0	107 ± 25	JCMT/SCUBA-2	7
850.0	5.7 ± 1.0	JCMT/SCUBA-2	7

References: (1) Hauck & Mermilliod (1998); (2) Perryman et al. (1997); (3) Skrutskie et al. (2006); (4) Egan et al. (2003); (5) Wright et al. (2010); (6) Ishihara et al. (2010); (7) This work; (8) Beichman et al. (1988).

the IRS spectrum in order to match the stellar photosphere model. This is in-line with typical scaling applied to calibrated IRS spectra (2 per cent to 7 per cent; Chen et al. 2014).

For inclusion in the SED fitting, flux densities were measured along the spectrum at wavelengths of 9, 13, 18, 24 and 31 μm. For each measurement the spectrum was averaged over all data points within 2 μm of the nominal wavelength. The IRS spectrum thus shows evidence for mid-infrared excess, strongly rising from the stellar photosphere at wavelengths beyond 20 μm.

2.2.2 *Far-infrared*

Herschel[2] (Pilbratt et al. 2010) Photometer Array Camera and Spectrograph (PACS; Poglitsch et al. 2010) scan-map observations of HD 76582 at 100 and 160 μm (Programme ot2_bzuckerm_2, P.I. Zuckerman) were obtained from the *Herschel* Science Archive. The *Herschel*/PACS images are presented in Fig. 1.

The individual scans were reduced interactively from the level 0 (raw data) products and mosaicked using the *Herschel* Interactive Processing Environment[3] (HIPE; Ott 2010) version 12, and PACS calibration version 65. We followed the reduction method adopted for the *Herschel* Open Time Key Programme 'Dust around Nearby Stars'; see Eiroa et al. (2013) for a detailed explanation. The data were high-pass filtered, with widths of 82 arcsec at 100 μm and 102 arcsec at 160 μm, to suppress large-scale background structure in the final images. Image scales of 1 arcsec per pixel at 100 μm and 2 arcsec per pixel at 160 μm were used in the final mosaics.

Flux densities were measured using aperture photometry, with appropriate aperture corrections applied to the measurement (taken from Balog et al. 2014) and background estimation via multiple sky apertures, again following Eiroa et al. (2013). We obtain flux density measurements of 609 ± 43 mJy at 100 μm, and 495 ± 35 mJy at 160 μm.

2.2.3 *Sub-millimetre*

The James Clerk Maxwell Telescope Sub-millimetre Common Use Bolometer Array (JCMT/SCUBA-2; Holland et al. 2013) 450 and 850 μm data for HD 76582 consist of five hours of observations taken in 10 half-hour chunks. The observations were taken using the constant speed DAISY pattern, providing uniform exposure time coverage of a region ∼3 arcmin in diameter centred on the target. The SCUBA-2 observations were reduced using the Dynamic Iterative Map-Maker within the STARLINK SMURF package (Chapin et al. 2013) called from the ORAC-DR automated pipeline (Cavanagh et al. 2008). The map maker configuration file was optimized for compact sources with a known position. A 'zero-masking' technique was applied to constrain the mean value of the map to zero beyond 60 arcsec from the centre of the field for all but the final iteration of the map-making process. This aided convergence of the iterative map-making and suppressed large-scale ringing artefacts. The data were high-pass filtered at 1 Hz (≡150 arcsec), removing large spatial scale noise. A final mosaic was created at each wavelength by co-adding the individual maps using inverse variance weighting. The mosaics have a scale of 1 arcsec per pixel. The mosaics have been smoothed with a 7 arcsec full width at half maximum (FWHM) Gaussian to improve the S/N. The images are presented in Fig. 2.

In the 450 μm image there is a clear peak, well-centred on the stellar position. The peak flux density is 89 ± 17 mJy beam^{-1}. Although the disc looks extended this is not significant. Negative 'holes' are visible in the map close to the target position, and complicate aperture photometry measurement (see Fig. 2). For a 12.5 arcsec radius aperture we obtain a flux density of 107 ± 25 mJy, consistent with the peak flux density measurement. At 850 μm there is a clear peak ∼3 arcsec offset from the stellar position. Such an offset is consistent with the magnitude of shifts expected for low S/N data, and much smaller than the beam FWHM (13 arcsec). The peak flux density is 5.8 ± 1.0 mJy beam^{-1}.

The observations of HD 76582 were obtained in two observing runs. From the first chunk of two hours of data, the disc is visible at 450 μm (188 ± 44 mJy), but not at 850 μm (3-σ < 4.8mJy). Such a result is unusual, as the greater sensitivity of JCMT/SCUBA-2 at 850 μm typically results in non-detection of debris discs at 450 μm. Furthermore, the slope of the sub-millimetre SED implied by this non-detection was far greater than the values obtained from previous detections or expected from theoretical considerations. Additional observations totalling three hours were acquired to determine the exact nature of the sub-millimetre excess, which resulted in the disc's detection at 850 μm, but also confirmed the steepness of the sub-millimetre slope, albeit less extreme than was measured in the initial observations.

[2] *Herschel* is an ESA space observatory with science instruments provided by European-led Principal Investigator consortia and with important participation from NASA.

[3] HIPE is a joint development by the Herschel Science Ground Segment Consortium, consisting of ESA, the NASA Herschel Science Center, and the HIFI, PACS and SPIRE consortia.

Downloaded from https://academic.oup.com/mnras/article-abstract/459/3/2893/2595210/Far-infrared-and-sub-millimetre-imaging-of-HD
by Cardiff University user
on 06 September 2017

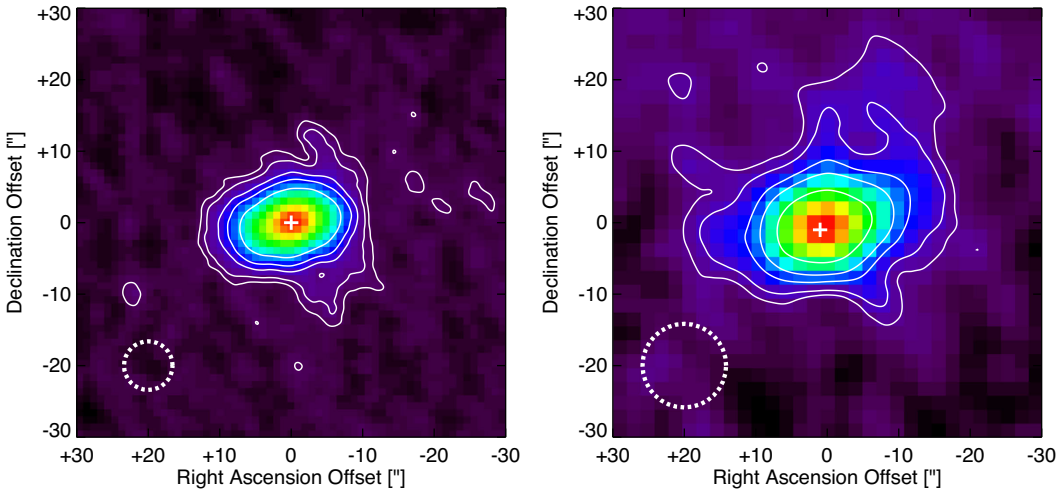

Figure 1. *Herschel*/PACS images of HD 76582 at 100 μm (left) and 160 μm (right). Stellar position is denoted by the white '+' symbol. Contours denote 3, 5, 10, 15, and 25-σ steps for a background r.m.s. of 0.07 mJy arcsec^{-2} at 100 μm and 0.15 mJy arcsec^{-2} at 160 μm. Image scale is 1 arcsec per pixel at 100 μm and 2 arcsec per pixel at 160 μm. Instrument beam FWHM is denoted by the dashed circle in the bottom left corner. Orientation is north up, east left.

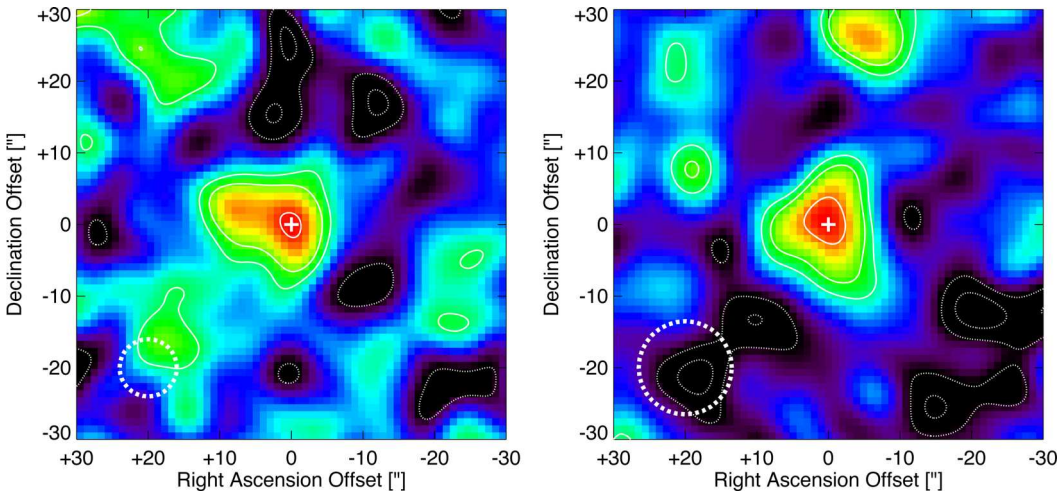

Figure 2. JCMT/SCUBA-2 images of HD 76582 at 450 μm (left) and 850 μm (right). The images have been smoothed with a 7 arcsec FWHM Gaussian. Stellar position is denoted by the white '+' symbol. Contours denote −3, −2, 2, 3, and 5-σ steps for a background r.m.s. of 0.306 mJy arcsec^{-2} at 450 μm and 0.005 mJy arcsec^{-2} at 850 μm. Image scale is 1 arcsec per pixel. Instrument beam is denoted by the dashed circle in the bottom left corner. Orientation is north up, east left.

3 SOURCE BRIGHTNESS PROFILES

We measured the source brightness profile along the major and minor axes in both *Herschel* bands as an additional constraint for the disc modelling process (see Fig. 3). To measure the profiles, the image was first rotated by an angle such that its major axis lay along the image x-axis. This rotated image was then interpolated to a grid 10 times finer than the image pixel scale (0.1 arcsec/0.2 arcsec per element at 100 μm/160 μm). The radial profile was measured from the peak of the source brightness profile to an extent of 30 arcsec at intervals equivalent to the pixel scale of the image (1 arcsec/2 arcsec at 100 μm/160 μm). The mean and standard deviation of two areas equidistant from the source peak along the x/y-axis were used to calculate the major/minor axis profile and its uncertainty, respectively.

To determine the disc extent, we follow the procedure laid out in Marshall et al. (2014b). A two-dimensional Gaussian is fitted to the source brightness profile in each image to estimate the source FWHM along the major and minor axes, $A_{\rm image}$ and $B_{\rm image}$, respectively, and the disc position angle, θ. The disc is then deconvolved from the instrument beam using a point spread function (PSF) standard, in this case an image of α Böotis, reduced in the same way as the images and rotated to the same orientation angle as the observations. The radially averaged FWHMs of the PSF are 6.8 arcsec at 100 μm and 11.3 arcsec at 160 μm. The deconvolved major and minor axis of the disc, $A_{\rm disc}$ and $B_{\rm disc}$ are then measured, again using a two-dimensional Gaussian profile. The disc is broader than the PSF along both axes in the PACS 100 μm images and the disc inclination is obtained from the deconvolved extent, i.e. $i = \cos^{-1}(B_{\rm disc}/A_{\rm disc})$. However in the PACS 160 μm images, the disc is only broader along the major axis and thus only marginally resolved in that waveband. A summary of the disc geometry and orientation derived from this analysis is presented in Table 3. The (minor) differences between the extent of the disc obtained here and in Vican et al. (e.g. lack of extended emission along the minor axis at 160 μm) could be due to the choice of α Boo rather than α Cet as a PSF standard.

Downloaded from https://academic.oup.com/mnras/article-abstract/459/3/2893/2595210/Far-infrared-and-sub-millimetre-imaging-of-HD
by Cardiff University user
on 06 September 2017

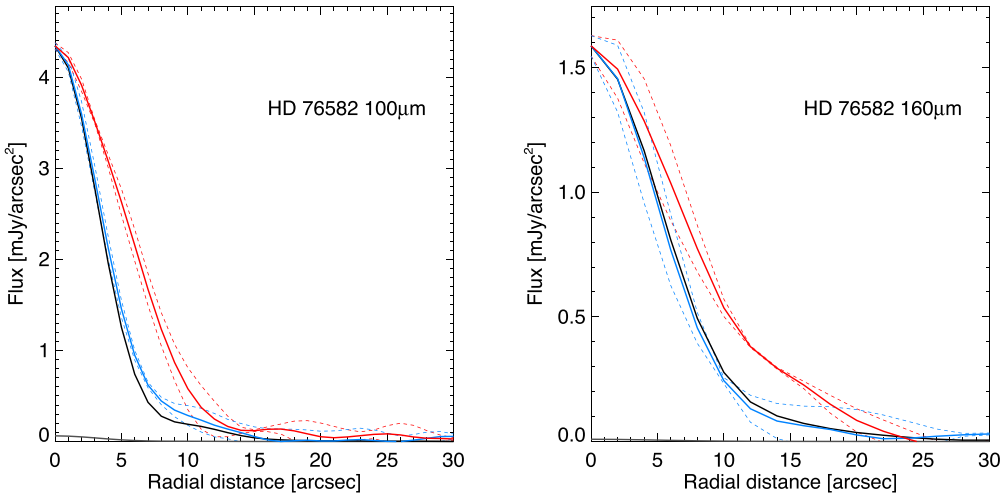

Figure 3. Radial profiles of HD 76582 at 100 μm (left) and 160 μm (right). The solid red line denotes the disc major axis, whilst the blue solid line denotes the minor axis; dashed lines of each colour represent the upper and lower bounds of the 1σ uncertainties. The grey line denotes a PSF scaled to the stellar photospheric contribution. The black line is a PSF scaled to the peak disc emission.

Table 3. Orientation and extent (FWHM or diameter) of the disc.

	HD 76582	
Parameter	100 μm	160 μm
$A_{\rm image}$ (arcsec)	11.8 ± 0.5	16.2 ± 0.7
$B_{\rm image}$ (arcsec)	8.0 ± 0.4	11.2 ± 0.5
PSF (arcsec)	6.8	11.3
$A_{\rm disc}$ (arcsec)	5.9 ± 0.1	8.5 ± 0.1
$A_{\rm disc}$ (au)	271 ± 10	391 ± 14
θ (°)	103 ± 5	115 ± 5
i (°)	64 ± 4	

Table 4. Results of modified blackbody fit to SED.

Parameter	Range	Distribution	Best fit
$T_{\rm inner}$ (K)	60–260	Linear	150 ± 20
$T_{\rm outer}$ (K)	30–60	Linear	44 ± 5
λ_0 (μm)	450	Fixed	450
β	0–2	Linear	1.9 ± 0.5
$L_{\rm IR}/L_\star$ ($\times 10^{-4}$)	n/a	Continuous	1.9 ± 0.3
$M_{\rm dust}$ ($\times 10^{-2} M_\oplus$)	n/a	Continuous	8.4 ± 1.4
$\chi^2_{\rm red}$	n/a	n/a	0.97

4 MODELLING

In the first instance we use a modified blackbody model to reproduce the observed excess from the circumstellar disc. Although not physically meaningful per se, this approach provides some guidance as to the number of debris components present in the system, and their location(s). We then apply those findings to constrain the parameter space explored by a power-law disc model that uses both the SED and images (radial profiles) in the fitting process.

4.1 Modified blackbody

The disc temperature derived from a blackbody fit to photometry up to 60 μm predicts a (minimum) dust semi-major axis of 43 au from the star, although more recent work by Pawellek et al. (2014) on resolved discs suggests the actual extent should be about twice this for a star of ∼10 $L_\odot$. The *Herschel*/PACS far-infrared images of HD 76582 at 100 and 160 μm presented here and in Vican et al. (submitted) show emission from a broad disc extending several hundred au from the star.

We attempt to replicate the shape of the disc SED with both one- and two-component modified blackbody models. The model is defined by a Planck function, $B(\nu, T_{\rm dust})$, for each component and a critical wavelength, λ_0, beyond which the Planck function is modified by a factor $(\lambda/\lambda_0)^{-\beta}$ reducing the flux density at wavelengths greater than λ_0. In both cases, the model is scaled to match the observed flux density at 100 μm.

A single-component modified blackbody cannot simultaneously replicate both the rise of the disc from the photosphere at mid-infrared wavelengths and the far-infrared excess/sub-millimetre slope. A two-component model replicates the observed excess satisfactorily, although not perfectly, across all wavelengths. This is indicative of either the presence of a single broad disc around HD 76582, or multiple physical components to the disc. The parameters of the best-fitting model are presented in Table 4, whilst the SED itself is shown in Fig. 4.

A simultaneous least-squares fit of two blackbodies to the excess at $\lambda \geq 20$ μm and S/N ≥ 3 was used to estimate the temperatures of the disc components. We find best-fitting temperatures of 150 ± 20 K for the inner component, and 44 ± 5 K for the outer component. In the blackbody approximation, these translate to separations of around 10 and 130 au, respectively. The fractional luminosities of the inner and outer components were 3×10^{-5} and 1.6×10^{-4}. Uncertainties were estimated from the shape of the χ^2 distribution by varying parameters individually whilst keeping the remainder fixed at the values of the best-fitting model. For the outer radius, this is close to the disc major axis derived from the extended emission in the *Herschel* images, $A_{\rm disc} = 271 \pm 10$au.

Due to the sparse coverage at sub-millimetre wavelengths, the break wavelength, λ_0, is poorly constrained by the modelling. We therefore fix λ_0 to 450 μm. Typically, λ_0 is taken as 210 μm; our adoption of a longer wavelength favours models with a warmer outer component leading to a larger β parameter to match the SED's slope between 450 and 850 μm. The β parameter itself, lying ∼2, is consistent with typical values for small dust grains in the interstellar medium, rather than those in circumstellar discs which would be closer to $\beta \sim 1$. A steep sub-millimetre slope usually signifies a disc whose SED is dominated by the smaller grains. In order to

Downloaded from https://academic.oup.com/mnras/article-abstract/459/3/2893/2595210/Far-infrared-and-sub-millimetre-imaging-of-HD
by Cardiff University user
on 06 September 2017

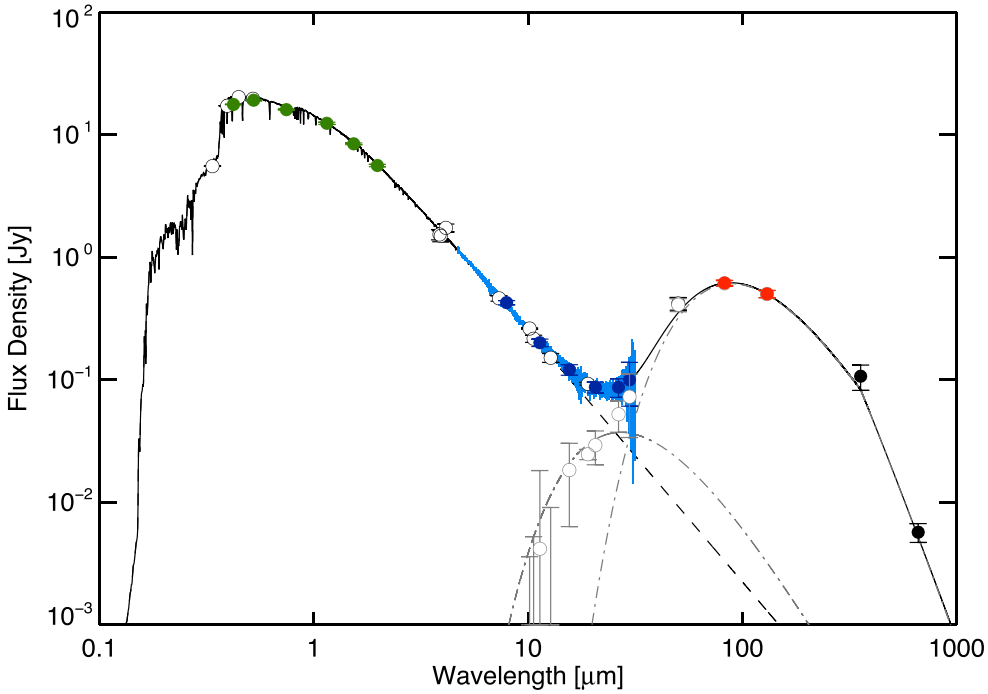

Figure 4. Two-component modified blackbody SED fit. Green denotes data used to scale the model stellar photosphere, light and dark blue denote the *Spitzer*/IRS spectrum and photometry, respectively, red denotes *Herschel*/PACS photometry, black denotes JCMT/SCUBA-2 photometry, white denotes literature data, and grey denotes photosphere-subtracted photometry. The dashed line is the stellar photosphere, the dot–dashed lines are the disc components, and the solid line is the combined star+disc model.

tally this with the agreement found between the imaged disc extent and the blackbody approximation from the SED we might invoke a large minimum grain size for the dust; this will be dealt with in the next section. A total disc fractional luminosity of 2.3×10^{-4} is calculated from the sum of the two components, slightly higher than, but comparable to, previous estimates (Moór et al. 2006).

An estimate for the dust mass in the disc can be obtained from the 850 μm flux density using the relation $M_{\rm dust} = F_{850} d^2 / \kappa_{850} B_{\nu, T_{\rm dust}}$ (e.g. Zuckerman & Becklin 1993; Najita & Williams 2005; Panić et al. 2013). Assuming a dust opacity of 1.7 gcm^{-2} (e.g. Pollack et al. 1994), a dust mass of $8.4 \pm 1.4 \times 10^{-2} M_{\oplus}$ is obtained for HD 76582's disc. This estimate is subject to large uncertainties due to the unknown dust grain properties such as emissivity, structure and size distribution, such that the dust mass derived here may be a factor of 3 to 5 lower than the actual value (Najita & Williams 2005).

4.2 Power law

Here, we approximate the disc with a power-law surface density (and size distribution), astronomical silicate dust model. We use the radiative transfer code SEDUCE (Müller, Löhne & Krivov 2010) to fit the SED. Model disc images were created based on the input parameters to the SED and convolved with an instrumental PSF for comparison with the *Herschel*/PACS images. In the least-squares fitting, a single image is given the same weight as a single photometric data point.

4.2.1 Single annulus disc

In the first instance, we attempt to replicate the outer disc with a single annulus. Whilst the SED is strongly suggestive of a multiple-component model, the disc is not well resolved such that a continuous disc should be investigated as a plausible architecture for the HD 76582 system. We account for the mid-infrared excess in this (and the next) model as an unresolved blackbody with a temperature of 150 K. The contribution of this component to the emission in *Herschel* images is small, with flux densities of 6 mJy at 100 μm and 2 mJy at 160 μm.

Table 5. Parameters of the single-component power-law disc model.

Parameter	Range	Distribution	Fit
R (au)	10–50	Linear	50 ± 5
ΔR (au)	10–250	Linear	170^{+40}_{-30}
α [−]	−5.0–2.0	Linear	$1.5^{+0.2}_{-0.5}$
$a_{\rm min}$ (μm)	0.5–50	Logarithmic	40±5
$a_{\rm max}$ (μm)	1000	Fixed	1000
γ [−]	3.0–7.0	Linear	$5.3^{+0.2}_{-0.4}$
$M_{\rm dust}$ ($\times 10^{-2} M_{\oplus}$)	n/a	Continuous	3.5
$\chi^2_{\rm red}$	n/a	n/a	13.25

The system geometry derived from the deconvolution process is adopted for the model architecture, fixing the inclination of the disc, i, as 64°, and the position angle, θ, at 103°. The disc extent is defined by its inner radius, R, width, ΔR, and radial surface density profile, α. The dust grains are assumed to be compact hard spheres composed of astronomical silicate (Draine 2003), whose size distribution is defined by an exponent γ ($dn \propto a^{-\gamma} da$) and ranges between $a_{\rm min}$ and 1 mm.

We find a good fit to the SED, shown in Fig. 6, the properties of which are summarized in Table 5 with a broad disc lying from 30 to 230 au with an outwardly increasing surface density profile of $\alpha = 1.5$. Whilst unusual, an outwardly increasing surface density profile

Downloaded from https://academic.oup.com/mnras/article-abstract/459/3/2893/2595210/Far-infrared-and-sub-millimetre-imaging-of-HD
by Cardiff University user
on 06 September 2017

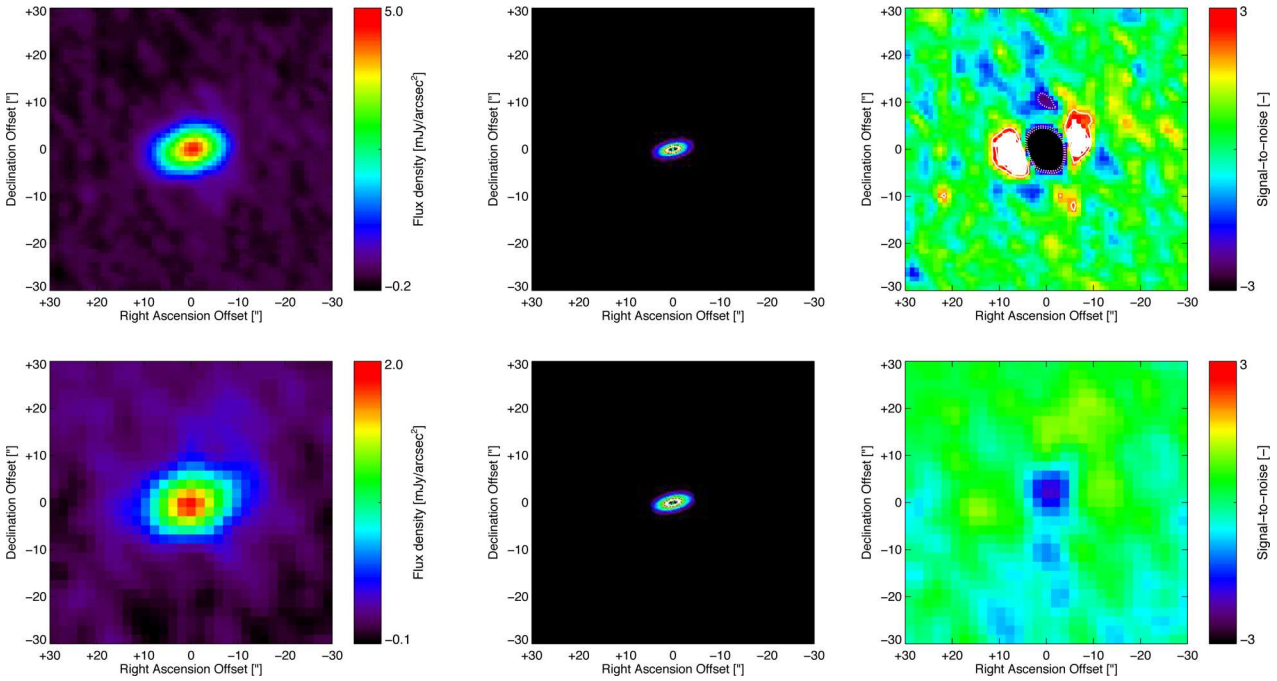

Figure 5. Broad disc model fit to the *Herschel*/PACS images at 100 μm (top) and 160 μm (bottom). The images show, from left to right, the observations, a high-resolution model of the disc, and the residuals after subtraction of the PSF-convolved models from the images. Contours in the residual images are $\pm 2\sigma$ and $\pm 3\sigma$, with broken contours denoting negative σ values. Significant residual flux is clearly visible in the 100 μm image.

is not unheard of amongst debris discs, e.g. AU Mic (MacGregor et al. 2013) and HD 107146 (Ricci et al. 2015). In order to replicate the lack of strong mid-infrared emission at $\lambda < 20\,\mu$m and the steep submillimetre slope of the SED, a large minimum grain size of 40 μm and steep particle size distribution exponent of $\gamma = 5.3$ are preferred in the model. The grain size is around 10 times the blow-out radius for the star ($a_{\rm blow} \sim 3.7\,\mu$m) which is a more typical result for later GK-type stars, whilst the steep size distribution implies that the disc emission is dominated by the smallest grains in the disc.

Although the SED is adequately matched by the single-component model, the 100 μm residual image, shown in Fig. 5, has a large amount of residual flux, at the $\geq 5\sigma$ level, in its outer regions, and suffers from over-subtraction in the inner regions. The peak of the residual flux lies at a separation of ∼250 au from the star, and is symmetric either side of the stellar position along the disc major axis. The presence of this residual emission is indicative that a two-component model is justified in fitting this disc, which we examine in the next section.

In Vican et al. (submitted) a single outer component with a radius of 210 au is used to replicate the extended emission in the *Herschel* PACS images. If a model that more heavily weights the disc structure over the SED in the fitting is adopted, we can replicate their findings. In this instance the SED is not well replicated, either having too narrow an excess at far-infrared wavelengths or too shallow a sub-millimetre slope, depending on the dust grain properties adopted. We therefore find that a single component for the outer disc is inadequate to the task of replicating all the available data.

4.2.2 *Multi-annular disc*

Following the results of the modified blackbody and power-law model, we model the outer disc using two annuli (i.e. a total of three belts present in the disc). As with the single annulus model, we use a blackbody component to account for the mid-infrared excess. In this instance the number of model parameters potentially outnumbers the number of data points, due to sparse sampling of the sub-millimetre SED, and the inner component of our disc model is only weakly constrained by the available data due to their low spatial resolution. To aid the modelling process we therefore make several simplifying assumptions regarding the properties of the disc.

First, we assume both annuli are narrow and co-planar, i.e. they have a width of 10 au and the same inclination and position angle. As per the broad disc model, the inclination, i, was assumed to be 64° and the position angle, θ, was fixed at 103°. Both annuli in the disc are defined by their radial distance (to inner edge of the annulus), $R_{\rm in}$ and $R_{\rm out}$, their widths, $\Delta R_{\rm in}$ and $\Delta R_{\rm out}$. Since the widths of the two components were fixed at 10 au, any investigation of the radial surface brightnesses, $\alpha_{\rm in}$ and $\alpha_{\rm out}$, is unmeaningful, hence these are also fixed as 0. The dust grain properties are defined by the minimum and maximum size of grains in the disc, $a_{\rm min}$ and $a_{\rm max}$, the power-law exponent of the particle size distribution, γ, and the dust composition (astronomical silicate; Draine 2003) with optical properties determined from Mie theory (e.g. Burns, Lamy & Soter 1979; Bohren & Huffman 1983). We assume that the grain size distribution is the same for both components, and the largest size of dust grains considered in the model is 1 mm. Finally, the slope of the particle size distribution, γ, is assumed to be the same for both components.

A two-component outer disc model adequately replicates both the SED and extended emission of this disc, as illustrated in Figs 7 and 8. We find that an outer disc comprising two narrow annuli at $R_{\rm in}$ = 80 au and $R_{\rm out}$ = 270 au adequately replicates the disc structure. For the dust properties, a minimum grain size of 10 μm for the 80 au annulus and 36 μm for the 270 au annulus is obtained; this result is tied to the need for the cooler (outer) annulus to match the steep

Downloaded from https://academic.oup.com/mnras/article-abstract/459/3/2893/2595210/Far-infrared-and-sub-millimetre-imaging-of-HD
by Cardiff University user
on 06 September 2017

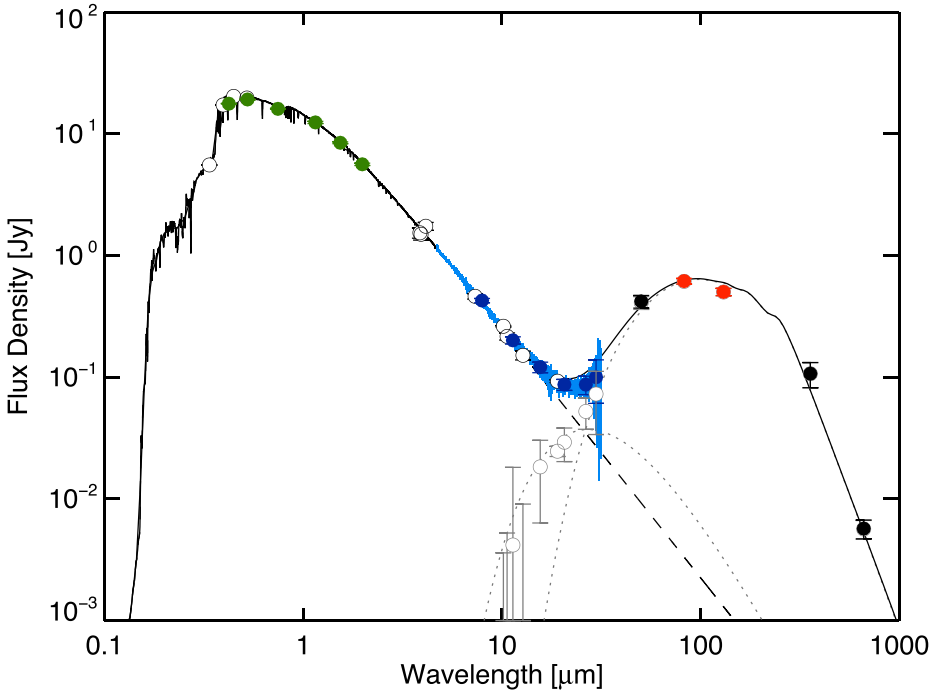

Figure 6. Single annulus power-law model + blackbody SED fit. Green denotes data used to scale the model stellar photosphere, light and dark blue denote the *Spitzer*/IRS spectrum and photometry, respectively, red denotes *Herschel*/PACS photometry, black denotes JCMT/SCUBA-2 photometry, white denotes literature data, and grey denotes photosphere-subtracted photometry. The dashed line is the stellar photosphere, the dot–dashed line is the disc contribution, and the solid line is the combined star+disc model.

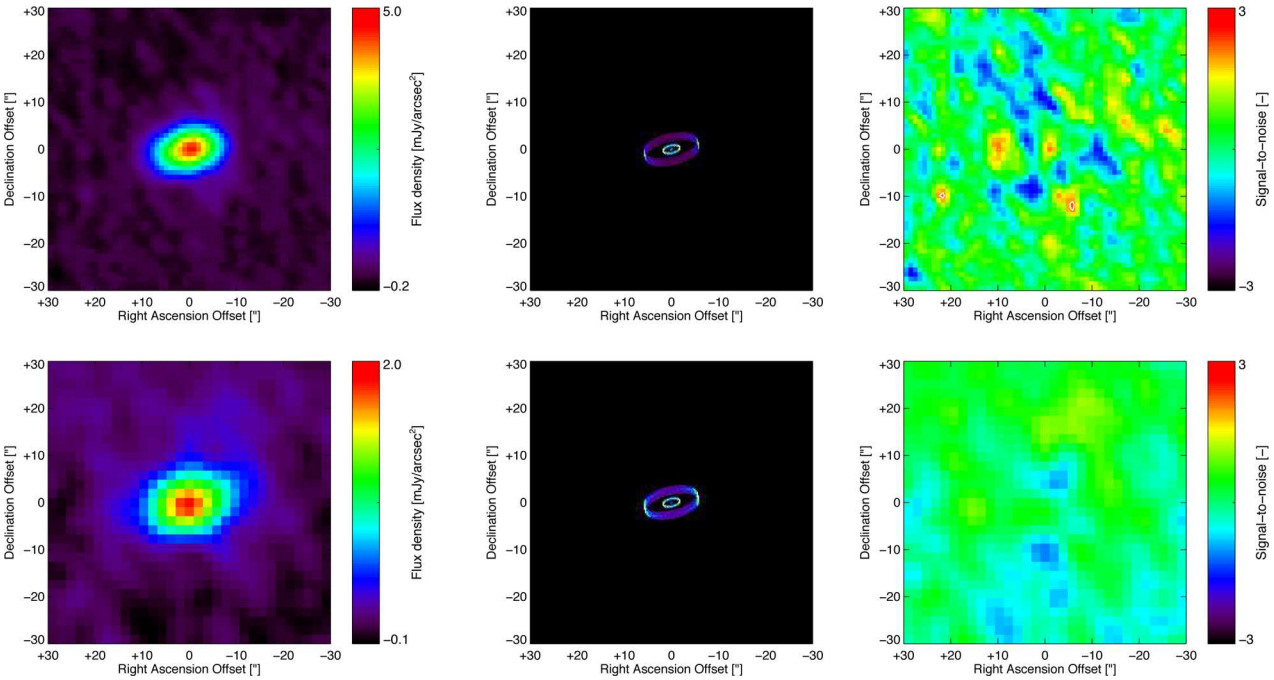

Figure 7. Multi-annular disc model fitted to the *Herschel*/PACS images at 100 μm (top) and 160 μm (bottom). The panels show, from left to right, the observed disc, a high-resolution two-ring disc model, the disc model convolved with the instrument PSF, and the residuals after subtraction of the convolved model from the observation. Contours in the residual images are $\pm 2\sigma$ and $\pm 3\sigma$, with broken contours denoting negative σ values.

sub-millimetre SED without contributing too strongly to the far-infrared part of the SED at 60 and 100 μm. The particle size distribution is again found to be significantly steeper than for a steady-state case with $\gamma = 5$ but this is also dictated by the sub-millimetre slope.

5 DISCUSSION

Our modelling of HD 76582's disc has shown evidence for three distinct physical components in the disc. Excesses at both mid- and far-infrared wavelengths, requiring disc components at two

Downloaded from https://academic.oup.com/mnras/article-abstract/459/3/2893/2595210/Far-infrared-and-sub-millimetre-imaging-of-HD
by Cardiff University user
on 06 September 2017

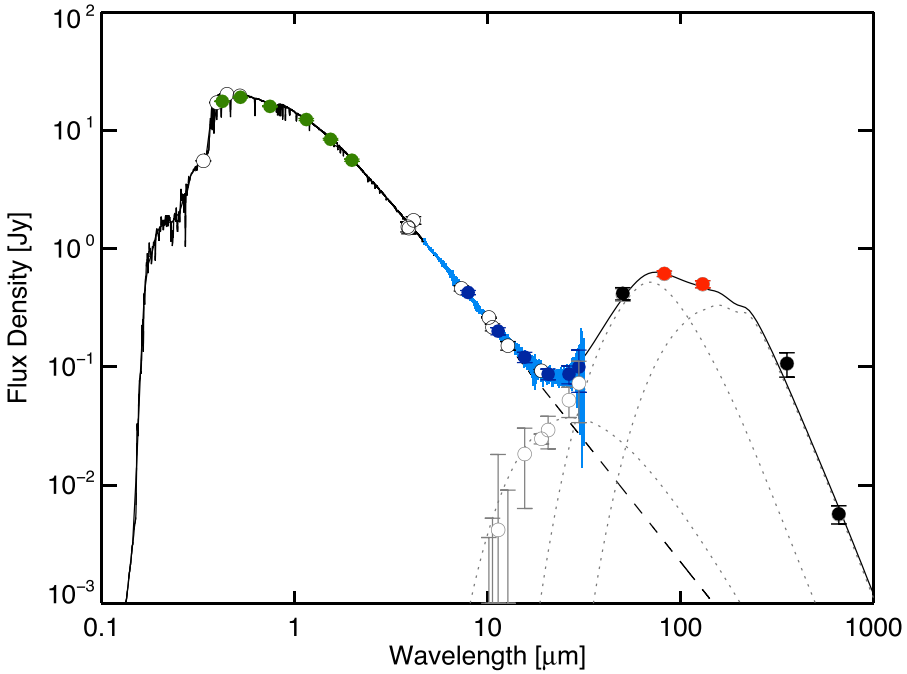

Figure 8. Two-component power-law model + blackbody SED fit. Green denotes data used to scale the model stellar photosphere, light and dark blue denote the *Spitzer*/IRS spectrum and photometry, respectively, red denotes *Herschel*/PACS photometry, black denotes JCMT/SCUBA-2 photometry, white denotes literature data, and grey denotes photosphere-subtracted photometry. The dashed line is the stellar photosphere, the dot–dashed lines are the disc components, and the solid line is the combined star+disc model.

Table 6. Parameters of the two-component power-law disc model.

	Range		Distribution	Fit	
Parameter	Inner	Outer		Inner	Outer
R (au)	10–100	100–300	Linear	80 ± 5	270^{+30}_{-10}
ΔR (au)	10		Fixed	10	
α	0.0		Fixed	0.0	
$a_{\rm min}$ (μm)	0.1–100.0		Logarithmic	10^{+2}_{-3}	36^{+4}_{-5}
$a_{\rm max}$ (μm)	1000		Fixed	1000	
γ	3.0–7.0		Linear	$5.0^{+0.5}_{-0.2}$	
$M_{\rm dust}$ ($\times 10^{-2} M_{\oplus}$)	n/a		Continuous	0.5	7.0
$L_{\rm IR}/L_{\star}$ ($\times 10^{-6}$)	n/a		Continuous	145	54
$\chi^2_{\rm red}$	n/a		n/a	2.45	

distinct temperatures, are often interpreted as evidence for physically distinct planetesimals belts in the disc (e.g. Morales et al. 2011, 2013; Kennedy & Wyatt 2014). As seen above, the disc's observational properties can be adequately replicated by a multi-annular architecture. However, a broad outer disc, over 150 au in extent, cannot replicate both the SED and the extended emission seen in the 100 μm *Herschel* images, and it would likewise be difficult to justify from a dynamical perspective. We therefore favour the multi-annular interpretation suggesting the outer disc structure has two distinct and physically separate components along with a spatially unresolved inner component. However, images with low spatial resolution provide little constraint to the inner parts of the system; a clear physical separation between the inner and outer system is not conclusively shown in these data. It might well be that the disc is a single contiguous structure around the star, but with several regions with different properties (as we expect a radial variation in the particle size distribution of dust). Multi-annular structures have previously been inferred in this manner for the debris discs around e.g. β Leo (Churcher et al. 2011), γ Dor (Broekhoven-Fiene et al. 2013), and HD 23484 (HIP 17439; Ertel et al. 2014).

The resolved outer disc extent is approximately twice the blackbody radial extent ($A_{\rm disc}/R_{\rm bb} = 2.08$). For a star of ∼10 $L_{\odot}$, the ratio of observed disc radius to blackbody radius, Γ, is expected to lie around 3.5 (fig. 10; Booth et al. 2013). Observations by *Herschel* show a range of values for Γ up to ∼2 (Booth et al. 2013; Pawellek et al. 2014). The disc therefore lies closer to the blackbody radius than theoretical expectations, suggesting that the dominant grains responsible for far-infrared emission are larger than the blow out radius ($a_{\rm blow} = 3.7$ μm) but not large enough to radiate as blackbodies. This result is consistent with the minimum grain size ($a_{\rm min} = 36$ μm) derived in the modelling process.

A typical particle size distribution exponent in the range 3 to 4 is inferred for those debris discs that have been detected at (sub-)millimetre wavelengths (Pan & Schlichting 2012; Ricci et al. 2015). Such values are consistent with a steady-state collisional cascade and expected values derived from collisional modelling (3.5 to 3.7; Dohnanyi 1969; Thébault & Augereau 2007; Gáspár et al. 2012). Here, we find an exponent of 5 is required to replicate the SED's sub-millimetre slope. This, in combination with the minimum grain size from the model $a_{\rm min}$ being 36 μm (for the outer disc), implies the disc (at least in its outer regions) is dominated by moderately sized dust grains. Such properties are reminiscent of the peculiar 'steep SED' debris discs detected at far-infrared wavelengths by Ertel et al. (2012), which have comparable ages (∼300 Myr) to that quoted for HD 76582 (at the lower end), and may therefore represent analogous systems to this one, albeit much fainter ($L_{\rm IR}/L_{\star} \sim$ a few $\times 10^{-6}$). For discs around luminous stars, the minimum grain size inferred from modelling tends to approach the blowout radius (Booth et al. 2013; Pawellek et al. 2014). The mid- and far-infrared excesses preclude the presence of small grains, below ∼10 μm, contributing to the observed emission as that would increase the disc brightness too

Downloaded from https://academic.oup.com/mnras/article-abstract/459/3/2893/2595210/Far-infrared-and-sub-millimetre-imaging-of-HD
by Cardiff University user
on 06 September 2017

much at wavelengths <100 μm. The minimum grain size inferred for the outer parts of this system is thus some three to 10 times larger than the blowout radius, 3.7 μm, derived from radiation pressure arguments (Burns et al. 1979).

The values of $a_{\rm min}$ in the outer disc derived from the astronomical silicate model are large (10 and 36 μm). This seems to contradict the high value for β found in fitting the modified blackbody model which would imply a large amount of small grains. Comparing the results from the astronomical silicate model, with large grains and a steep size distribution, and the modified blackbody model, with the high beta value, both point towards a disc where its emission is being dominated by the smallest grains. For a more typical disc, a shallower size distribution (in the astronomical silicate model) would broaden the shape of the far-infrared excess and decrease the beta value (for the modified blackbody case). These modelling outcomes can be reconciled by noting that the grains simply need to be inefficient emitters to replicate the sub-mm slope, and that the observed emission is dominated by the smallest grains in the disc (which may not necessarily be small themselves).

A further avenue of investigation is the adoption of a different material for the disc's constituent dust grains. Given the broad parameter space opened by relaxing the condition of a single (pure astronomical silicate) dust composition it is not unreasonable to expect that some combination of materials (and porosity) such as water ice might replicate the disc SED. However, the modelling process is limited such that any multi-material composition found to replicate the SED in this way would exceed the number of available free parameters. That being said, diligence requires us to address that possibility here. We may attempt to fit the SED using dust grains of different properties whilst keeping the constraint of the disc architecture derived from fitting the images. Three alternative materials to astronomical silicate are considered: amorphous water ice (Li & Greenberg 1998), 'dirty ice' (Preibisch et al. 1993), and graphite (Jager, Mutschke & Henning 1998). The optical constants for these materials were taken from the Jena data base.[4] We found that none of the materials could replicate the SED with an appreciably shallower size distribution or smaller minimum grain size than the results obtained for astronomical silicate grains, and we therefore do not devote any further efforts to presentation of these results. Whilst this approach is non-exhaustive, it demonstrates that the disc properties calculated in this work are not a quirk of adopting standard assumptions regarding the dust grain properties.

Given its unusual properties, we may consider the evolutionary state of the disc; is it actually in a state of flux, or are its properties consistent with a steady-state evolution? To do this, we compare the fractional luminosity of HD 76582's disc to the models presented in Wyatt et al. (2007), whereby the maximum brightness, $f_{\rm max}$, for a disc around an A star of a given age can be calculated, under certain assumptions (their equations 14 and 20). HD 76582's disc has fractional luminosities of 3.1×10^{-5} for the warm disc (blackbody), and 1.45×10^{-4} and 5.4×10^{-5} for the two annuli in the cool disc. Adopting a separation of $r_{\rm in} = 20$ au for the blackbody component, and $r_{\rm mid} = 80$ au and $r_{\rm out} = 270$ au for the outer two components we can consider these regions separately. Given an age of 0.45 Gyr, $f_{\rm max,in}$ is 1.8×10^{-5}, whereas for an age of 2.13 Gyr, $f_{\rm max,in}$ is 3.9×10^{-6}. For the outer system, at 0.45 Gyr $f_{\rm mid,max} = 1.1 \times 10^{-4}$ and $f_{\rm out,max} = 5.9 \times 10^{-4}$, whereas at 2.13 Gyr $f_{\rm mid,max} = 2.5 \times 10^{-5}$ and $f_{\rm out,max} = 1.2 \times 10^{-4}$. Given the large uncertainties on the calculation of $f_{\rm max}$ (Wyatt et al. 2007), this does not conclusively show that the system is brighter than expected for steady-state collisional evolution. Nonetheless, taken together with the steep dust size distribution and large minimum grain size, this does leave open the possibility that HD 76582's disc is not in a quiescent state and is in the process of some dynamical upheaval revealed through its unusual dust emission. The outermost parts of the disc still having a brightness compatible with steady-state evolution would be expected with this scenario as the collisional time-scales will be greater there.

A further issue in examining the state of HD 76582's disc is the evolutionary state of the host star. As an F0 IV sub-giant, the star is undergoing mass loss via a strong stellar wind. The impact of stellar winds on debris discs on the main sequence has been investigated in Mizusawa et al. (2012), where no difference in excess detection rate between early and late F-type stars was seen, suggesting the stellar winds had little impact on the circumstellar debris. Around sub-giant stars, discs have been examined by e.g. Bonsor et al. (2013, 2014). For these post-main-sequence discs (Bonsor & Wyatt 2010) calculated that the disc survives the evolution process but the increased luminosity of the evolved host is more effective at removing smaller grains through radiation pressure. However, the impact of the stellar wind on the disc was negligible over the range of systems studied, as per the main sequence.

In the case of HD 76582, the multi-annular structure of the disc suggests the presence of massive, unseen bodies in the intervening gaps. As a host star undergoes mass loss on the giant branch, the semi-major axes of companion bodies will expand outwards by a factor of two to three in the adiabatic case (Mustill & Villaver 2012; Mustill, Veras & Villaver 2014). An exoplanet (or large planetesimals) migrating outward in this fashion would stir the planetesimal belts, brightening the disc through increased dust production from collisions. As a subgiant, the amount of mass loss from HD 76582 is small and the impact of this on the orbits of circumstellar bodies would therefore be modest.

To resolve the issue of the disc structure satisfactorily, further high angular resolution images are required. Two obvious approaches are through (sub-)mm interferometry or scattered light imaging at optical/near-infrared wavelengths. However, the HD 76582 system presents a challenge in this regard. In the case of sub-mm follow up, the precipitous drop of the sub-mm excess reduces the integrated flux for the disc to 1.1 mJy at 1300 μm. Confining this flux to be spread in two annuli within a radial extent of ∼6 arcsec, and assuming a beam FWHM of 1.5 arcsec (to separate the two outer annuli), requires a total of 10 beams to cover the disc area. An observation with S/N ∼10 beam^{-1} is feasible with currently available facilities, such as ALMA. The case for scattered light imaging is more difficult, despite the disc being relatively bright, as the conversion between thermal and scattered excess is highly uncertain (Schneider et al. 2014). The large minimum grain size inferred by our model also counts against the feasibility of such a measurement as comparably bright discs with such large grains have been found to be difficult to image (see e.g. Krist et al. 2010, 2012).

6 CONCLUSIONS

We present the first sub-millimetre detection of the debris disc around HD 76582, along with spatially resolved far-infrared images. Measurement of the spectral slope at 450 and 850 μm reveals a steep fall-off of the disc SED at sub-millimetre wavelengths inconsistent with values observed, and predicted, for typical discs. We combine these new observations with available photometry and

[4] http://www.astro.uni-jena.de/Laboratory/OCDB/

Downloaded from https://academic.oup.com/mnras/article-abstract/459/3/2893/2595210/Far-infrared-and-sub-millimetre-imaging-of-HD
by Cardiff University user
on 06 September 2017

images at far-infrared wavelengths to constrain the disc's geometry and extent, and the dust grain properties in a self-consistent model that simultaneously fits all available data. HD 76582's disc has a position angle of 103° and an inclination of 64°. The disc modelling favours three physically separate components: an unresolved component at ∼20 au responsible for the mid-infrared excess, and two annuli at 80 and 270 au responsible for the far-infrared excess. The steep size distribution, $\gamma = 5.0$, large minimum grain size, $a_{\rm dust}$ >10 μm, and fractional luminosity of the disc, $L_{\rm IR}/L_\star = 2.3 \times 10^{-4}$, lead us to infer that we do not observe the HD 76582 system in a steady state.

ACKNOWLEDGEMENTS

We thank the referee for improving the paper with their helpful comments. JPM is supported by a UNSW Vice-Chancellor's Postdoctoral Research Fellowship. MB acknowledges support from FONDECYT Postdoctral Fellowships, project no. 3140479, and the Millennium Science Initiative (Chilean Ministry of Economy), through grant Nucleus P10-022-F. This research has made use of the SIMBAD data base, operated at CDS, Strasbourg, France. This research has made use of NASA's Astrophysics Data System. This paper is based on data obtained by the JCMT Debris Disc Legacy Survey, Program ID MJLSD02. The James Clerk Maxwell Telescope has historically been operated by the Joint Astronomy Centre on behalf of the Science and Technology Facilities Council of the United Kingdom, the National Research Council of Canada and the Netherlands Organisation for Scientific Research. Additional funds for the construction of SCUBA-2 were provided by the Canada Foundation for Innovation.

REFERENCES

Allende Prieto C., Lambert D. L., 1999, A&A, 352, 555
Ammler-von Eiff M., Reiners A., 2012, A&A, 542, A116
Backman D. E., Paresce F., 1993, in Levy E. H., Lunine J. I., eds, Protostars and Planets III. Univ. Arizona Press, p. 1253
Balog Z. et al., 2014, Exp. Astron., 37, 129
edsBeichman C. A., Neugebauer G., Habing H. J., Clegg P. E., Chester T. J. 1988, Infrared Astronomical Satellite (IRAS) Catalogs and Atlases. Volume 1: Explanatory Supplement Vol. 1. Washington D.C.
Bohren C. F., Huffman D. R., 1983, Absorption and Scattering of Light by Small Particles. Wiley, New York
Bonsor A., Wyatt M., 2010, MNRAS, 409, 1631
Bonsor A., Kennedy G. M., Crepp J. R., Johnson J. A., Wyatt M. C., Sibthorpe B., Su K. Y. L., 2013, MNRAS, 431, 3025
Bonsor A., Kennedy G. M., Wyatt M. C., Johnson J. A., Sibthorpe B., 2014, MNRAS, 437, 3288
Booth M. et al., 2013, MNRAS, 428, 1263
Broekhoven-Fiene H. et al., 2013, ApJ, 762, 52
Burns J. A., Lamy P. L., Soter S., 1979, Icarus, 40, 1
Castelli F., Kurucz R. L., 2004, preprint (astro-ph/0405087)
Cavanagh B., Jenness T., Economou F., Currie M. J., 2008, Astron. Nachr., 329, 295
Chapin E. L., Berry D. S., Gibb A. G., Jenness T., Scott D., Tilanus R. P. J., Economou F., Holland W. S., 2013, MNRAS, 430, 2545
Chen C. H., Mittal T., Kuchner M., Forrest W. J., Lisse C. M., Manoj P., Sargent B. A., Watson D. M., 2014, ApJS, 211, 25
Churcher L. J. et al., 2011, MNRAS, 417, 1715
David T. J., Hillenbrand L. A., 2015, ApJ, 804, 146
De Rosa R. J. et al., 2014, MNRAS, 437, 1216
Dohnanyi J. S., 1969, J. Geophys. Res., 74, 2531
Dominik C., Decin G., 2003, ApJ, 598, 626
Draine B. T., 2003, ApJ, 598, 1017
Egan M. et al., 2003, Air Force Research Laboratory Technical Report AFRL-VS-TR-2003-1589, p. 1
Eggleton P. P., Tokovinin A. A., 2008, MNRAS, 389, 869
Eiroa C. et al., 2013, A&A, 555, A11
Ertel S. et al., 2012, A&A, 541, A148
Ertel S. et al., 2014, A&A, 561, A114
Gáspár A., Psaltis D., Rieke G. H., Özel F., 2012, ApJ, 754, 74
Giridhar S., Goswami A., Kunder A., Muneer S., Selvakumar G., 2013, A&A, 556, A121
Hauck B., Mermilliod M., 1998, A&AS, 129, 431
Holland W. S. et al., 2013, MNRAS, 430, 2513
Houck J. R. et al., 2004, in Mather J. C., ed., Society of Photo-Optical Instrumentation Engineers (SPIE) Conf. Ser. Vol. 5487, Optical, Infrared, and Millimeter Space Telescopes. Society of Photo-Optical Instrumentation Engineers, p. 62
Hughes A. M., Wilner D. J., Andrews S. M., Williams J. P., Su K. Y. L., Murray-Clay R. A., Qi C., 2011, ApJ, 740, 38
Ishihara D. et al., 2010, A&A, 514, A1
Jager C., Mutschke H., Henning T., 1998, A&A, 332, 291
Kennedy G. M., Wyatt M. C., 2014, MNRAS, 444, 3164
Krist J. E. et al., 2010, AJ, 140, 1051
Krist J. E., Stapelfeldt K. R., Bryden G., Plavchan P., 2012, AJ, 144, 45
Krivov A. V., 2010, Res. Astron. Astrophys., 10, 383
Krivov A. V., Müller S., Löhne T., Mutschke H., 2008, ApJ, 687, 608
Lebouteiller V., Barry D. J., Spoon H. W. W., Bernard-Salas J., Sloan G. C., Houck J. R., Weedman D. W., 2011, ApJS, 196, 8
Lestrade J.-F., Thilliez E., 2015, A&A, 576, A72
Li A., Greenberg J. M., 1998, A&A, 331, 291
Lowrance P. J. et al., 2000, ApJ, 541, 390
MacGregor M. A. et al., 2013, ApJ, 762, L21
Marshall J. P. et al., 2014a, A&A, 565, A15
Marshall J. P. et al., 2014b, A&A, 570, A114
Matthews B. C., Krivov A. V., Wyatt M. C., Bryden G., Eiroa C., 2014, Protostars and Planets VI, Univ. Arizona Press, p. 521
Mizusawa T. F., Rebull L. M., Stauffer J. R., Bryden G., Meyer M., Song I., 2012, AJ, 144, 135
Moór A., Ábrahám P., Derekas A., Kiss C., Kiss L. L., Apai D., Grady C., Henning T., 2006, ApJ, 644, 525
Morales F. Y., Rieke G. H., Werner M. W., Bryden G., Stapelfeldt K. R., Su K. Y. L., 2011, ApJ, 730, L29
Morales F. Y., Bryden G., Werner M. W., Stapelfeldt K. R., 2013, ApJ, 776, 111
Moro-Martín A. et al., 2015, ApJ, 801, 143
Müller S., Löhne T., Krivov A. V., 2010, ApJ, 708, 1728
Mustill A. J., Villaver E., 2012, ApJ, 761, 121
Mustill A. J., Veras D., Villaver E., 2014, MNRAS, 437, 1404
Najita J., Williams J. P., 2005, ApJ, 635, 625
Neugebauer G. et al., 1984, ApJ, 278, L1
Ott S., 2010, in Mizumoto Y., Morita K.-I., Ohishi M., eds, ASP Conf. Ser. Vol. 434, Astronomical Data Analysis Software and Systems XIX. Astron. Soc. Pac., San Francisco, p. 139
Pan M., Schlichting H. E., 2012, ApJ, 747, 113
Panić O. et al., 2013, MNRAS, 435, 1037
Pawellek N., Krivov A. V., Marshall J. P., Montesinos B., Ábrahám P., Moór A., Bryden G., Eiroa C., 2014, ApJ, 792, 65
Perryman M. A. C. et al., 1997, A&A, 323, L49
Pilbratt G. L. et al., 2010, A&A, 518, L1
Poglitsch A. et al., 2010, A&A, 518, L2
Pollack J. B., Hollenbach D., Beckwith S., Simonelli D. P., Roush T., Fong W., 1994, ApJ, 421, 615
Preibisch T., Ossenkopf V., Yorke H. W., Henning T., 1993, A&A, 279, 577
Rhee J. H., Song I., Zuckerman B., McElwain M., 2007, ApJ, 660, 1556
Ricci L., Carpenter J. M., Fu B., Hughes A. M., Corder S., Isella A., 2015, ApJ, 798, 124
Schneider G. et al., 2014, AJ, 148, 59
Skiff B. A., 2014, VizieR Online Data Catalog, 1, 2023
Skrutskie M. F. et al., 2006, AJ, 131, 1163
Su K. Y. L. et al., 2013, ApJ, 763, 118
Thébault P., Augereau J.-C., 2007, A&A, 472, 169
Thureau N. D. et al., 2014, MNRAS, 445, 2558

Downloaded from https://academic.oup.com/mnras/article-abstract/459/3/2893/2595210/Far-infrared-and-sub-millimetre-imaging-of-HD
by Cardiff University user
on 06 September 2017

van Leeuwen F., 2007, A&A, 474, 653
Vitense C., Krivov A. V., Kobayashi H., Löhne T., 2012, A&A, 540, A30
Werner M. W. et al., 2004, ApJS, 154, 1
Wittenmyer R. A., Marshall J. P., 2015, AJ, 149, 86
Wright E. L. et al., 2010, AJ, 140, 1868
Wyatt M. C., 2003, ApJ, 598, 1321
Wyatt M. C., 2008, ARA&A, 46, 339
Wyatt M. C., Smith R., Su K. Y. L., Rieke G. H., Greaves J. S., Beichman C. A., Bryden G., 2007, ApJ, 663, 365
Zorec J., Royer F., 2012, A&A, 537, A120
Zuckerman B., Becklin E. E., 1993, ApJ, 414, 793
Zuckerman B., Song I., 2004a, ARA&A, 42, 685
Zuckerman B., Song I., 2004b, ApJ, 603, 738

This paper has been typeset from a TEX/LATEX file prepared by the author.

Downloaded from https://academic.oup.com/mnras/article-abstract/459/3/2893/2595210/Far-infrared-and-sub-millimetre-imaging-of-HD
by Cardiff University user
on 06 September 2017